


ARTICLE

DOI: 10.1038/s41467-018-05412-0

OPEN

Regulation of T cell afferent lymphatic migration by targeting LT β R-mediated non-classical NF κ B signaling

Wenji Piao¹, Yanbao Xiong^{1,2}, Konrad Famulski ³, C. Colin Brinkman^{1,2}, Lushen Li^{1,2}, Nicholas Toney¹, Chelsea Wagner^{1,2}, Vikas Saxena^{1,2}, Thomas Simon^{1,2} & Jonathan S. Bromberg^{1,2,4}

Lymphotoxin-beta receptor (LT β R) signaling in lymphatic endothelial cells (LEC) regulates leukocyte afferent lymphatic transendothelial migration (TEM). The function of individual signaling pathways for different leukocyte subsets is currently unknown. Here, we show that LT β R signals predominantly via the constitutive and ligand-driven non-classical NIK pathway. Targeting LT β R-NIK by an LT β R-derived decoy peptide (nciLT) suppresses the production of chemokines CCL21 and CXCL12, and enhances the expression of classical NF κ B-driven VCAM-1 and integrin β 4 to retain T cells on LEC and precludes T cell and dendritic cell TEM. nciLT inhibits contact hypersensitivity (CHS) at both the sensitization and elicitation stages, likely by inhibiting leukocyte migration. By contrast, targeting LT β R-classical NF κ B signaling during the elicitation and resolution stages attenuates CHS, possibly by promoting leukocyte egress. These findings demonstrate the importance of LT β R signaling in leukocyte migration and LEC and lymphatic vessel function, and show that antagonist peptides may serve as lead compounds for therapeutic applications.

¹Center for Vascular and Inflammatory Diseases, University of Maryland School of Medicine, Baltimore, MD 21201, USA. ²Department of Surgery, University of Maryland School of Medicine, Baltimore, MD 21201, USA. ³Department of Laboratory Medicine and Pathology, University of Alberta, 250 Heritage Medical Research Centre, Edmonton, AB T6G 2S2, Canada. ⁴Department of Microbiology and Immunology, University of Maryland School of Medicine, Baltimore, MD 21201, USA. These authors contributed equally: Wenji Piao, Yanbao Xiong. Correspondence and requests for materials should be addressed to J.S.B. (email: jbromberg@som.umaryland.edu)

Recirculating CD4 T cells enter lymph nodes (LNs) from tissues via afferent lymphatics or from blood across high endothelial venules (HEV). Transendothelial migration (TEM) of the leukocytes from blood to LNs or blood to non-lymphoid tissues has been extensively studied¹. Alternatively, the regulation of T cell migration from tissues to LNs via afferent lymphatics is far less well defined. Recent studies from this and other laboratories suggest that mechanisms of afferent lymphatic T cell migration are distinct from those used by DC, neutrophil, or monocyte migration, in that T cell migration is governed by integrin-independent mechanisms, such as S1P/S1PR1-mediated homeostatic T cell trafficking² and LT α 1 β 2/lymphotoxin-beta receptor (LT β R)-mediated regulatory T cells (Treg) entry into lymphatics³.

The migration of Treg from grafts to LN via afferent lymphatics is critical for graft survival, and cannot be supplanted by Treg migration from blood through HEV into the same LN⁴. Treg specifically employ several molecular mechanisms, distinct from non-Treg CD4⁺ T cells, to migrate through afferent lymphatics^{3,5}. A unique mechanism employed by Treg is the high level expression of cell surface lymphotoxin (LT), which is required for migration from the allograft to afferent lymphatics and then to the draining LN³. This LT-dependent mechanism is neither required to enter LN via the HEV, nor for egress from the LN to efferent lymphatics. Treg cell surface LT binds to and activates the LT β receptor (LT β R) expressed on lymphatic endothelial cells (LEC), causing changes in LEC morphology that accompany Treg migration.

LT is a member of the tumor necrosis factor (TNF) superfamily that has major role in lymphoid organogenesis^{6,7}. LT has two subunits (LT α and LT β) and is found in two distinct forms: soluble homotrimer of LT α (LT α 3) that binds TNF receptors, and membrane-bound heterotrimer (LT α 1 β 2) that signals via LT β receptor (LT β R) (shown in Fig. 1e). Unlike TNF receptors (TNFR) that exclusively activate the classical arm of NF κ B, LT β R activation induces both the classical and non-classical NF κ B pathways⁸. The classical NF κ B activation is rapid and transient, involves the Inhibitor of kappa-B kinase (IKK)-complex mediated phosphorylation and degradation of the inhibitor I κ B α causing the release of RelA/p50 complex and transfer to the nucleus to allow inflammatory gene transcription. In contrast, activation of non-classical NF κ B is gradual and involves NF κ B inducing kinase (NIK)-dependent processing of p100 into its transcription-regulatory fragment p52 that dimerizes with RelB and results in nuclear translocation. The recruitment of adaptor protein TNFR-associated factor (TRAF) 2 and 3 to LT β R triggers NF κ B signal pathways. For LT β R-mediated p100 processing in LT α β -activated cells, TRAF2 bridges cellular inhibitors of apoptosis (cIAP) 1/2, an E3 ubiquitin ligase, to degrade TRAF3. TRAF3-deficient cells exhibit constitutive p100 processing. TRAF2 and TRAF3 thus function as mediators and inhibitors of LT β R signaling, respectively^{9–11}.

Classical IKK β -NF κ B-dependent genes include inflammatory chemokines (CCL4 and CCL2) and adhesion molecules (VCAM-1, ICAM-1, and ELAM-1). In contrast, alternative IKK α -RelB/p52-dependent genes include homeostatic chemokines involved in lymphoid organogenesis (CCL19, CCL21, and CXCL12)^{12,13}. The Treg LT α β -LEC LT β R interaction favors the non-classical over the classical signaling pathway^{3,14}. However, the precise nature of LT β R signaling in LEC and the consequences for LEC structure and function that regulate leukocyte migration remain to be fully defined and quantitated.

LT β Rlg, a soluble decoy fusion protein comprised of the ectodomain of LT β R fused to Fc of immunoglobulin G, blocks LT/LIGHT binding to LT β R and has shown efficacy in preclinical disease models as an anti-inflammatory treatment¹⁵. However,

these results have not been consistent across disease models^{16,17}. As LT β Rlg blocks signaling induced by both LT α 1 β 2 and LIGHT, and blocks both the classical and non-classical NF κ B pathways, it is difficult to determine which ligands and signaling pathways are important in the various models. Thus, specific targeting of individual arms of LT β R signaling should reveal the pathway that is responsible for promoting leukocyte trafficking, and enable selective control of leukocyte migration.

Herein we use LT β R-specific cell permeable peptides to selectively target separate arms of the NF κ B pathway and reveal the molecular mechanism of leukocyte migration. The results show that constitutive and stimulated afferent LEC LT β R signaling preferentially engage the NIK pathway, resulting in changes in LEC morphology, structure, and gene expression. These NIK-induced effects couple with T cell ligands and receptors to determine TEM into the afferent lymphatics. The results reveal a general requirement for LEC LT β R NIK signaling for normal afferent lymphatic migration of leukocytes. These findings suggest how lymphatic migration may be regulated in homeostasis and during the induction and resolution of inflammatory events.

Results

LT β R mediates non-classical NF κ B signaling in LEC. Flow cytometry, immunohistochemistry, and western blot analysis of murine primary LEC, the SVEC4-10 LEC line, and lymphatic vessels *in vivo* confirmed that LEC express high levels of the LT β R (Fig. 1a, b). Although agonist anti-LT β R mAb induced early classical NF κ B activation in LEC with weak phosphorylation of IKK α / β or I κ B α degradation, TNF α -induced strong IKK α / β phosphorylation and I κ B α degradation in the same cells (Fig. 1c), showing that classical and rapid NF κ B signaling were intact. Notably, LT β R activation induced nuclear translocation of RelA, which is the essential subunit of classical NF κ B (Fig. 1d, e), showing that the classical pathway was indeed induced through LT β R. In contrast, agonist anti-LT β R mAb mediated strong NIK signaling as indicated by increased p100 processing into p52, and p100 processing was further strengthened by crosslinking the agonist antibody (Fig. 1c). AT406, an inhibitor of cIAP1/2, the E3 ubiquitin ligase which targets NIK for proteasome-mediated degradation in resting cells, promoted more LT β R-mediated NIK accumulation and p100 processing in LEC and SVEC4-10 (Fig. 1e, f), further confirming the activation of the NIK signaling pathway by LT β R activation. It was noteworthy that NIK expression was observed in resting primary LEC and SVEC4-10 and in Lyve-1-expressing LEC of mouse ear pinnae *in vivo* (Fig. 1b), and at baseline there were low levels of p52 present in the LEC and SVEC4-10 (Fig. 1c, f). Furthermore, LT β R and NIK co-localized in LEC confocal images (Fig. 1b). Together, these data suggested that there is low-level constitutive activation of the non-classical pathway in LEC both *in vivo* and *in vitro*, and preferential induction of the non-classical pathway by LT β R signaling.

LT β R induces chemotactic molecules by both pathways. LT β R ligation on LECs induced VCAM-1 and the inflammatory chemokine CCL2 transcription as early as 3 h after stimulation (Fig. 2a), along with increasing cell surface VCAM-1 (Fig. 2b, c) and CCL2 secretion (Fig. 2d). Crosslinking anti-LT β R mAb on the cell surface to potentiate receptor signaling further enhanced CCL2 transcription (Fig. 2a). LT β R-mediated CCL2 production and VCAM-1 expression were suppressed by BAY11-7085, an irreversible inhibitor of I κ B α phosphorylation (Fig. 2b, d). In contrast, the NIK inhibitor 4H-isoquinoline-1, 3-dione (NIKi) did not affect VCAM-1 expression on LEC. These results

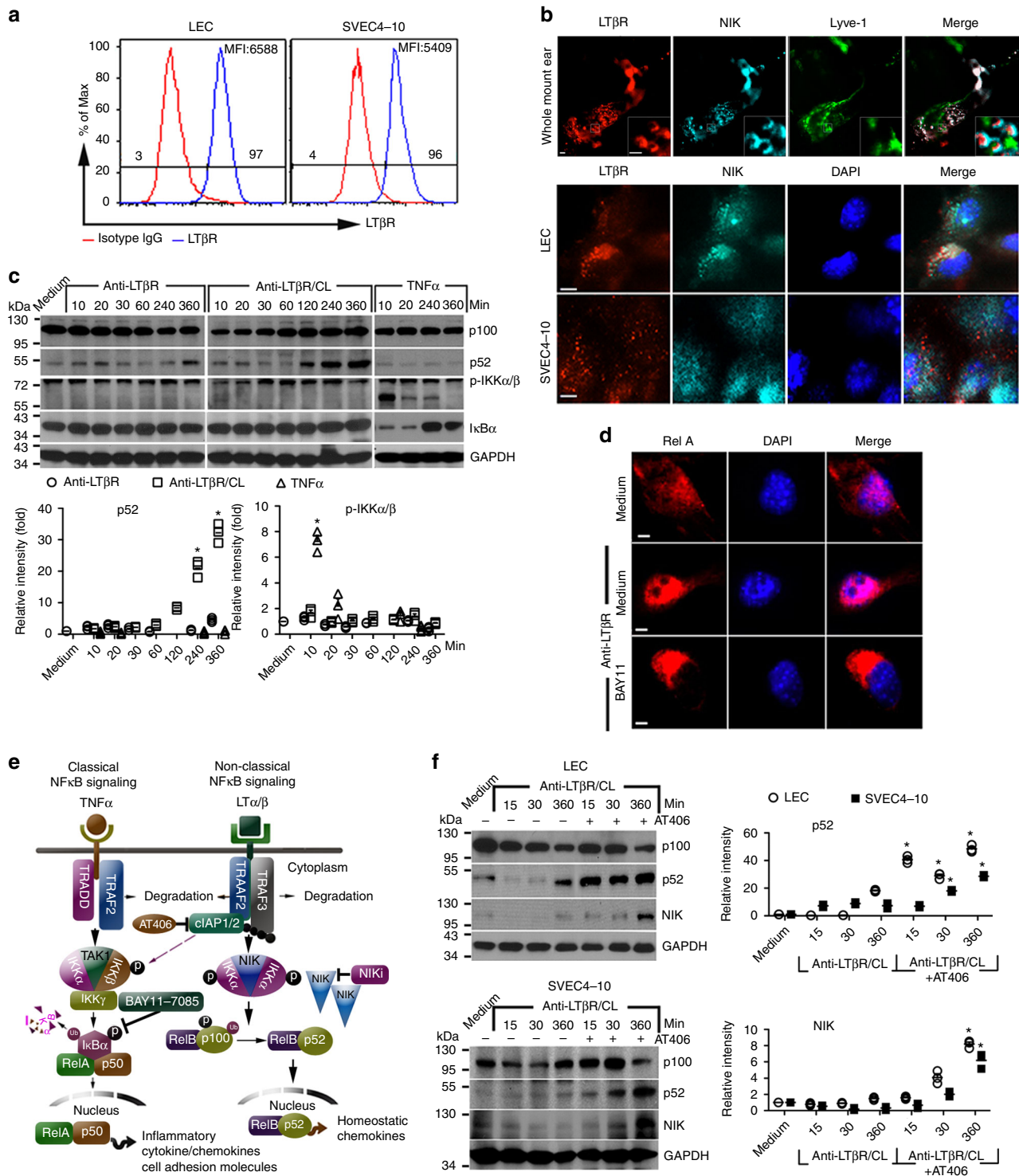


Fig. 1 Preferential non-classical NFκB signaling induced by LTβR activation in LEC. **a** Flow cytometry analysis of LTβR expression on murine primary LEC and SVEC4-10. MFI mean fluorescence intensity. **b** Immunohistochemistry of LTβR and NIK expression on mouse whole-mount ear, primary LEC, and SVEC4-10. Magnification ×20, ×60 (inset); scale bar 10 μm. **c** Mouse primary LEC stimulated with 2 μg/mL 3C8 anti-LTβR mAb or 20 ng/mL TNFα for the indicated times. For crosslinking (CL), cells incubated with 2 μg/mL anti-LTβR mAb at 4 °C, washed, and then crosslinked with 2 μg/mL mouse anti-rat IgG1 for the indicated times. Cell lysates immunoblotted for p100, p52, phosphorylated IKKα/β, IκBα, and GAPDH. The bar graphs represent the relative band intensities (mean ± SEM) from three independent experiments. *p < 0.05 by one-way ANOVA. **d** Nuclear translocation of RelA/p65 in LEC stimulated with 2 μg/mL anti-LTβR for 10 min. Magnification ×60; scale bar 4 μm. **e** Diagram of TNFα and LTβR-mediated classical and non-classical NFκB signaling. **f** Mouse primary LEC or SVEC4-10 treated as in **c**, along with 25 μM AT406. Cell lysates immunoblotted for p100, p52, NIK, and GAPDH. The bar graphs represent the relative band intensities (mean ± SEM) from three independent experiments. *p < 0.05 by one-way ANOVA

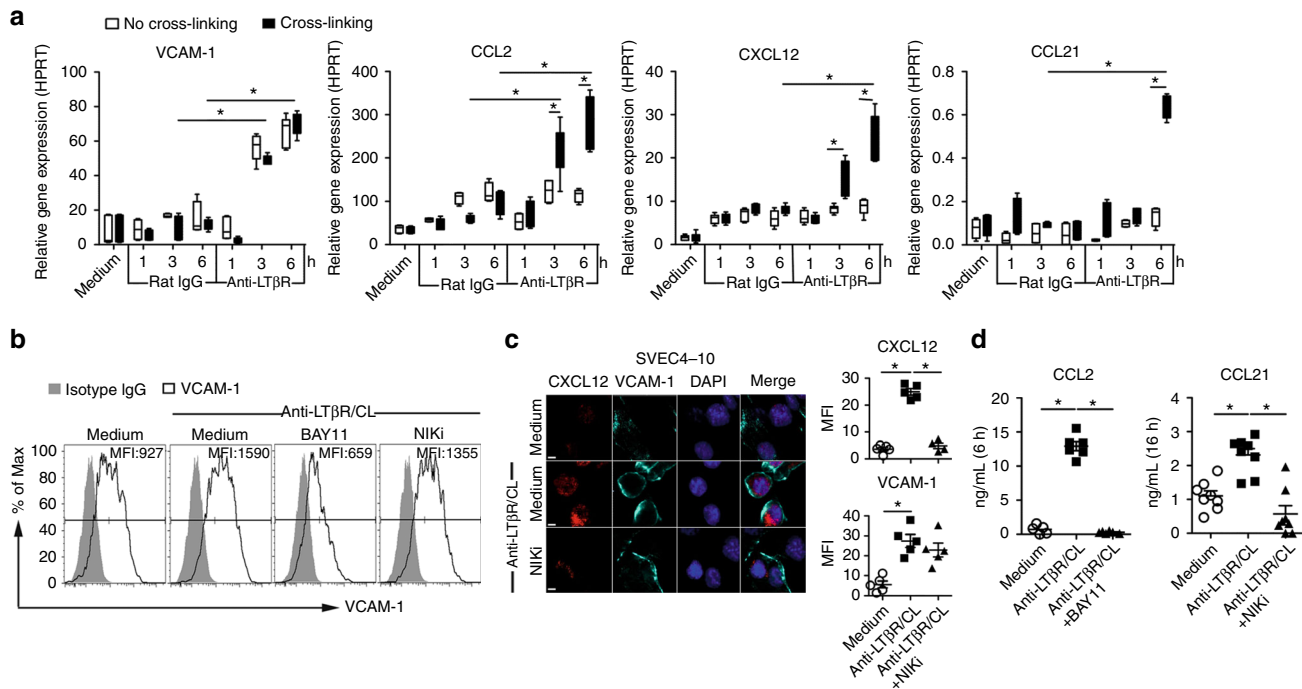


Fig. 2 Agonistic anti-LT β R mAb induces inflammatory and homeostatic chemokines and cell adhesion molecules in LEC. **a** qRT-PCR of indicated genes induced by agonistic anti-LT β R mAb or isotype rat IgG crosslinked with or without mouse anti-rat IgG1 in LEC at the indicated times. Treated as in Fig. 1. **b** Flow cytometry analysis of VCAM-1 expression on LEC after treatment with anti-LT β R mAb plus crosslinking, with or without 25 μ M NF κ B inhibitor BAY11-7085 or 50 μ M NIKi for 3 h. **c** LT β R-induced CXCL12 and VCAM-1 expression on SVEC4-10 treated with anti-LT β R mAb plus crosslinking, with or without NIKi (50 μ M) for 3 h. Magnification $\times 60$; scale bar 5 μ m. **d** Secretion of CCL2 and CCL21 by LEC stimulated with anti-LT β R mAb plus crosslinking, with or without BAY11-7085 (25 μ M) or NIKi (50 μ M) measured at the indicated times. * $p < 0.05$ by one-way ANOVA (**a**, **d**) or by Student's *t*-test (**c**)

confirmed the dependence of CCL2 and VCAM-1 expression on the classical NF κ B pathway.

Transcription of the homeostatic chemokines CXCL12 and CCL21 gradually peaked 6 h after strong LT β R stimulation induced by crosslinking the agonist mAb (Fig. 2a), and CCL21 secretion was detectable after 16 h (Fig. 2d). Increased intracellular CXCL12 and CCL21 could also be demonstrated after anti-LT β R mAb crosslinking on LEC (Fig. 2a, c, d). CXCL12 and CCL21 production induced by LT β R activation were inhibited by the NIKi (Fig. 2c, d), confirming the non-classical pathway dependence of the expression of these genes. Together, these results showed that LT β R stimulation on LEC resulted in the earlier expression of genes regulated by the classical NF κ B pathway followed by the later expression of genes regulated by the non-classical NIK pathway, and suggested differences in LT β R requirements for weak or strong signals.

LT β R-derived peptides that target separate NF κ B pathways.

LT β R recruits TNF receptor-associated factors (TRAFs) 2, 3, and 5 via its intracellular domain. Mutagenesis studies indicate that TRAF binding to specific motifs in LT β R bifurcates the two arms of NF κ B signaling (Fig. 3a)^{18,19}. To regulate separate LT β R signaling pathways, we designed decoy peptides comprised of the N-terminal cell-penetrating sequence of the *Drosophila* antennapedia peptide (RQIKIWFQNRRMKWKK) plus one of the TRAF-binding motifs in LT β R to specifically target each arm of the NF κ B pathway (Fig. 3a). nciLT(RQIKIWFQNRRMKWKKKTGNIYIYNGPVL) harbored the sequence required for TRAF2 and TRAF3 recruitment into the activated, non-classical LT β R complex and p100 processing¹⁸. ciLT (RQIKIWFQNRRMKWKKTPEEGAPGP) included the (P/S/A/T)X (Q/E)E TRAF-binding motif required for TRAF2 but not TRAF3

binding to LT β R in the classical pathway^{18,20}. A control peptide (RQIKIWFQNRRMKWKKGEHGQVAHGA) included the random sequence of LT β R amino acids. The effective doses and incubation periods for the peptides were determined by cytokine (CCL2, CCL21, CXCL12) and receptor (VCAM-1) mRNA expression responses of SVEC4-10 maximally activated by crosslinking of agonist anti-LT β R mAb and treated with various doses of nciLT and ciLT (Supplementary Fig. 1). The results showed that a concentration of 20 μ M of each peptide gave optimal results, similar to our previous experience with peptides of different specificities^{21,22}.

To evaluate their blocking activities in signaling responses, LEC were incubated with these blocking peptides prior to activation with anti-LT β R mAb, and compared to conventional, receptor nonselective inhibitors of the separate NF κ B signaling pathways. With respect to classical signaling in LEC and SVEC4-10 cells, TRAF3 constitutively bound to the LT β R, and LT β R activation induced rapid TRAF2 recruitment to the receptor after 10 min (Fig. 3b) followed by later TRAF2 degradation after 6 h (Fig. 3c). Immunoprecipitation showed that ciLT but not BAY11-7085 was sufficient to inhibit both TRAF2 and TRAF3 precipitating with the LT β R complex (Fig. 3b), either by preventing binding to and/or inducing dissociation from the receptor. ciLT but not BAY11-7085 also prevented TRAF2 degradation (Fig. 3c). These results indicated that ciLT acted as an inhibitor of the LT β R upstream classical NF κ B pathway, while BAY11-7085 acted as a downstream inhibitor of the classical NF κ B receptor/TRAF complex. In keeping with the low level of classical NF κ B activities induced by the LT β R in these cells (Fig. 1c), there was no observed LT β R-induced rapid phosphorylation of IKK α / β or I κ B, or I κ B degradation in LEC and SVEC4-10 (Fig. 3d). Nonetheless, nuclear translocation of RelA and early response genes of the classical pathway (CCL2,

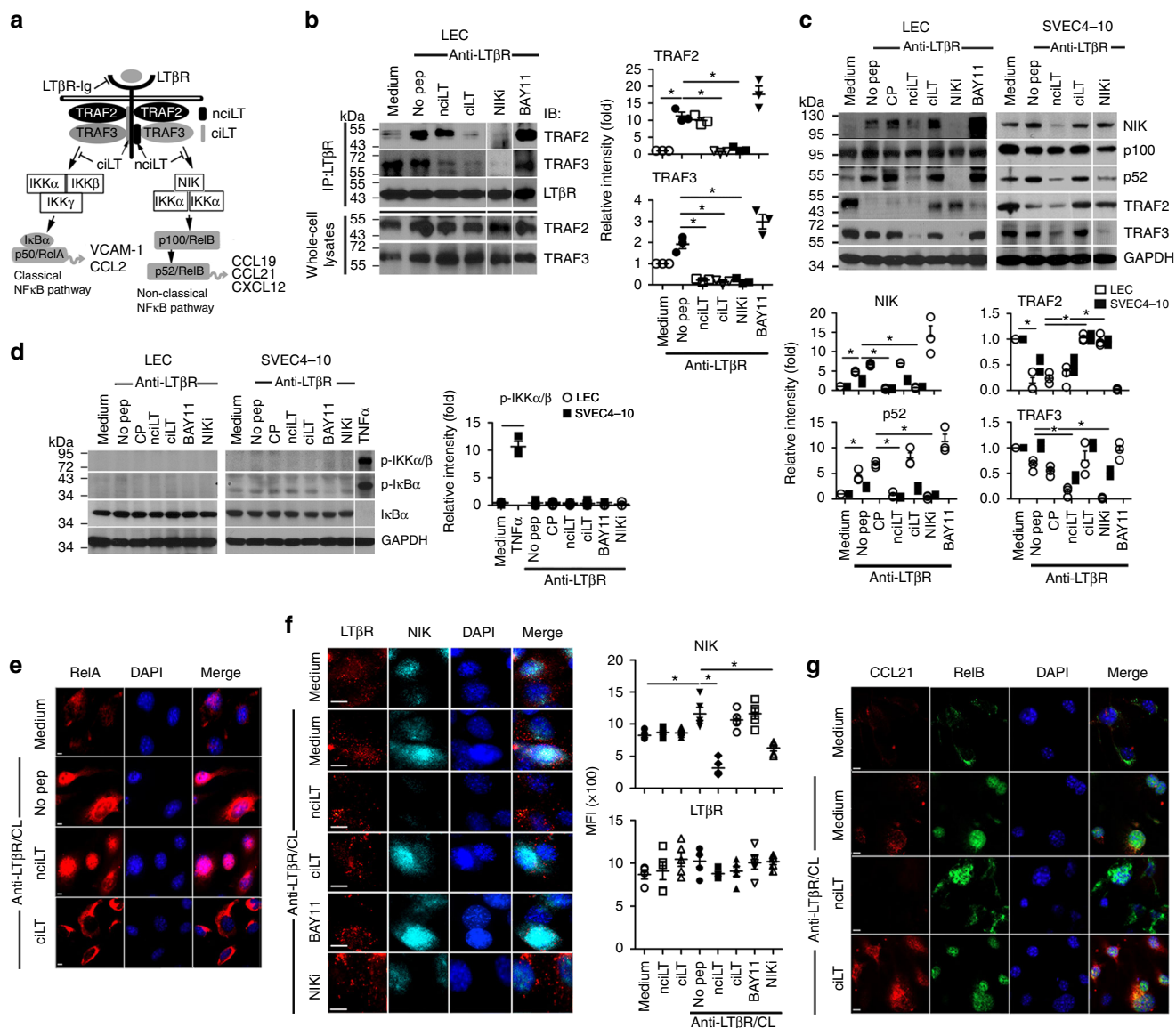


Fig. 3 Targeting of LTβR-mediated classical and non-classical NFκB signaling pathways by LTβR-specific peptides. **a** Diagram of peptide selective blockade of separate arms of LTβR signaling. **b** Immunoprecipitation of LTβR complex with anti-LTβR in lysates of LEC pretreated with the indicated peptides (20 μM) and then stimulated with anti-LTβR mAb (2 μg/mL) for 10 min. Complexes run on SDS-PAGE, and immune blotted with anti-TRAF2, anti-TRAF3, and anti-LTβR. **c, d** LEC and SVEC4-10 pretreated with indicated peptides (20 μM) or inhibitors (25 μM BAY11-7085; 50 μM NIKi) and then stimulated with anti-LTβR (2 μg/mL) for 6 h (**c**) or 10 min (**d**). In panel **d**, SVEC4-10 stimulated with 20 ng/mL TNFα. Cell lysates immune blotted for p100, p52, NIK, TRAF2, and TRAF3 (**c**); for IKKα/β, and for IκBα phosphorylation and degradation (**d**). **e** Cells treated as in (**d**); immunohistochemistry of RelA. Magnification ×60; scale bar 4 μm. **f, g** Cells treated as in (**c**). Immunohistochemistry of LTβR and NIK in SVEC4-10 (**f**); CCL21 and RelB in LEC (**g**). Magnification ×60; scale bar 8 μm (**f**) or 4 μm (**g**). The bar graphs in (**b-d**) represent the relative band intensities (mean ± SEM) from three independent experiments. **p* < 0.05 by one-way ANOVA

VCAM-1) were induced by LTβR activation and the translocation and gene expression were specifically inhibited by ciLT (Fig. 3e, Supplementary Fig. 1).

With respect to the non-classical pathway, activation of LTβR in LEC and SVEC4-10 induced rapid and strong NIK accumulation followed by p100 processing to p52 (Fig. 3c, f). Notably, there was TRAF3 binding to LTβR in unstimulated LECs (Fig. 3b) suggesting, as noted above (Fig. 1b, c, e), low level constitutive activation of the non-classical pathway via the LTβR. Immunoprecipitation showed that nciLT blocked TRAF3 but not TRAF2 binding to the LTβR complex (Fig. 3b) and prevented p100 processing to p52 (Fig. 3c). In comparison, NIKi blocked both TRAF2 and TRAF3 recruitment to the receptor, prevented

downstream p100 processing to p52, and inhibited TRAF2 degradation. These results showed that nciLT specifically sequestered TRAF3 from the receptor complex, and did not prevent TRAF2 degradation, but did prevent NIK accumulation for non-classical NFκB signaling. In contrast, NIKi prevented TRAF2 degradation, which is required for classical NFκB activation, suggesting NIK was a more specific NIK pathway inhibitor than NIKi. In fact, NIKi had a partial inhibitory effect on CCL2 transcription activated by the classical pathway (Supplementary Fig. 2). Late response genes of the non-classical pathway (CCL21, CXCL12) were induced by LTβR activation and their expression was specifically inhibited by nciLT (Supplementary Fig. 1).

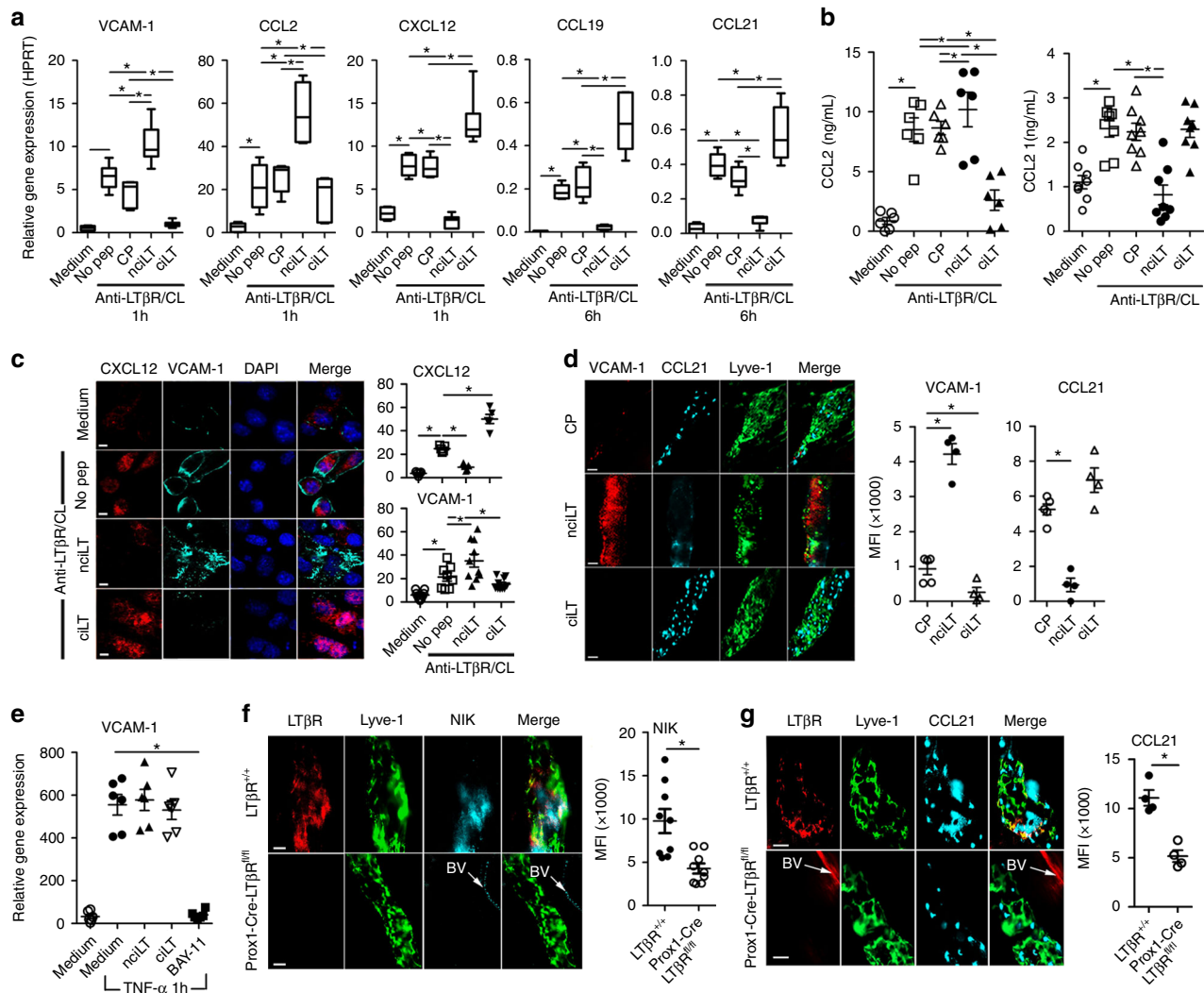


Fig. 4 Regulation of gene profiles by the LT β R NF κ B-blocking peptides. **a** qRT-PCR of VCAM-1 and chemokines in LEC stimulated with anti-LT β R mAb (2 μ g/mL) plus CL with mouse anti-rat IgG1 (2 μ g/mL) for the indicated times. **b** ELISA for CCL2 and CCL21 in the LEC supernatants after 4 or 16 h stimulation as in **a**, respectively. **c** CXCL12 and VCAM-1 expression in LEC after 3 h stimulation as in **a**. Magnification $\times 40$; scale bar 20 μ m. **d** C57BL/6 mice injected with 5 nmol/ear control peptide (CP), nciLT or ciLT; after 3 h ears were fixed for whole-mount ear staining. Magnification $\times 20$; scale bar 50 μ m. **e** qRT-PCR of VCAM-1 in LEC stimulated with TNF α (20 ng/mL) for 1 h. **f, g** Whole-mount ear staining of NIK and CCL21 in Prox1-Cre-ER^{T2} $^{-/-}$ LT β R^{fl/fl} mice 10 days after tamoxifen treatment (0.125 mg/g i.p. for 5 consecutive days). BV blood vessel. Magnification $\times 60$; scale bar 10 μ m. $^*p < 0.05$ by one-way ANOVA (**a–e**) or by Student's *t*-test (**f, g**)

Immunohistochemistry showed co-expression of LT β R and NIK on LEC and SVEC4-10, with co-localization of the two molecules in confocal images (Figs. 1b, 3f). nciLT and NIKi inhibited NIK expression and its co-localization with LT β R, without affecting LT β R expression (Fig. 3f). In contrast, neither ciLT nor BAY11-7085 affected NIK expression or co-localization with LT β R. In addition, LT β R activation induced RelB nuclear translocation which was suppressed by nciLT but not ciLT (Fig. 3g). Together, these data confirmed the specificity and mechanism of activity of nciLT in comparison to the other three molecules.

Gene profiles are regulated by LT β R-NF κ B-blocking peptides.

To further validate the peptide inhibitor specificities and mechanisms, their actions were related to the separate LT β R signaling pathways and specific gene activation. The blocking peptides were assessed for their effects on early classical pathway and later non-classical pathway gene activation and expression in LEC. nciLT, which blocked LT β R-non-classical NF κ B signaling, enhanced early

classical pathway CCL2 and VCAM-1 expression and inhibited homeostatic CXCL12, CCL19, and CCL21 chemokine production via the non-classical pathway, as measured by RT-PCR (Fig. 4a), ELISA (Fig. 4b), and immunohistochemistry (Fig. 4c). nciLT was also effective in vivo and significantly decreased the expression of CCL21 and increased VCAM-1 expression on Lyve-1⁺ lymphatic vessels (Fig. 4d). Conversely, ciLT blockade of the LT β R-classical NF κ B pathway suppressed classical pathway induced CCL2 and VCAM-1 and enhanced non-classical homeostatic chemokines CXCL12, CCL19, and CCL21 (Fig. 4a–d). Both peptides showed LT β R-specific inhibition since TNFR1-mediated VCAM-1 expression was not affected by either nciLT or ciLT, yet was significantly inhibited by BAY11-7085 (Fig. 4e). Thus, these peptides specifically inhibited gene expression regulated by the classical and non-classical pathways engaged by LT β R. Selective deletion of LT β R in Prox1-expressing lymphatics 10 days after tamoxifen treatment of Prox1-Cre-ER^{T2} $^{-/-}$ LT β R^{fl/fl} mice also diminished NIK and CCL21 expression (Fig. 4f, g), confirming the importance of LT β R and NIK signaling.

Targeting non-classical signaling inhibits T cell migration. We previously demonstrated that CD4⁺ Treg but not CD4⁺ non-Treg utilized cell surface LT α β to engage LT β R on LEC to migrate across the afferent lymphatic endothelium *in vitro* and *in vivo*. Treg expressed higher levels of LT α β than non-Treg, and modulated membrane and cytoskeletal structure of LECs via LT β R-mediated NIK signaling³. To further investigate the roles of the separate signaling pathways, we evaluated the functional efficacy of the blocking peptides on Treg migration. *In vitro* transmigration assays showed that when LEC but not Treg were pretreated with blocking peptides, that nciLT prevented Treg TEM across LEC (Fig. 5a, left panel). In contrast, pretreatment of LEC with ciLT, the classical pathway blocking peptide, enhanced Treg migration, likely by modulating the expression of migration molecules regulated by the non-classical pathway, such as increased CCL21 and CXCL12 expression (Fig. 4a–d). The peptides did not affect LEC viability or permeability as shown by the MTT viability and Evans Blue barrier assays, respectively (Fig. 5b, c). Thus, migration inhibition was not due to non-specific effects on LEC viability or permeability. When LEC were incubated with peptides and then washed, the effect of the peptides persisted for more than 6 h prior to the migration assay, and were reversed by 12–16 h (Supplementary Fig. 3a).

nciLT also inhibited TEM of activated and naive CD4⁺ non-Treg T cells across LEC (Fig. 5a, middle and right panels). Our previous work demonstrated that additional engagement and activation of LT β R was required for TEM of Treg but not other T cells. The biochemical and immunohistochemical analyses showed that there was constitutive LT β R-NIK expression and activation in LEC, with TRAF3 occupancy (Fig. 3b, c) along with low levels of p52 (Fig. 1f). The current results showed that other T cells required the constitutive activation of LEC LT β R and LT β R-NIK signaling for TEM. Thus, nciLT likely inhibited constitutive receptor activity required for all CD4 T cell TEM. When LEC were specifically activated for 16 h with anti-LT β R mAb plus cross-linking, this resulted in increased migration of naive CD4 T cells (Fig. 5d), showing that receptor signaling and migration could be enhanced beyond constitutive receptor activation.

We observed similar effects on T cell migration *in vivo*. Injection of nciLT into the footpad inhibited naive CD4 T cell homing into local draining LNs, while ciLT injection increased the migration (Fig. 5e). Injection of stimulatory anti-LT β R mAb into the footpad enhanced migration, and this enhanced migration was blocked by nciLT (Fig. 5f). Injection of nciLT also inhibited CD4 T cells from entering into the lymphatic vessels in the ear pinna assay (Fig. 5g). These results confirmed the role for LT β R signaling and the NIK pathway for afferent lymphatic migration *in vivo* in both basal and stimulated conditions. Once injected into the footpads, the effects of the peptides persisted more than 20 h prior to the migration assay, and were reversed by 36 h (Supplementary Fig. 3b).

NIK inhibition enhances T cell binding to LEC. We also noted that treatment of LEC with nciLT resulted in markedly increased firm attachment of the LEC to the culture surfaces compared to untreated, control peptide treated, or ciLT-treated LEC. This was true both for resting LEC and LEC in which the LT β R was stimulated with the agonist mAb, again showing that LT β R-NIK constitutive and induced signaling were important for LEC layer structure. Given the observation of increased LEC adhesion, and the decreased T cell migration noted above (Fig. 5a, e, f), we questioned if there were also alterations in T cell adhesion to LEC. Live 2-D migration imaging showed that the CD4 T cells were tethered on nciLT-treated LEC, with significantly lower motility as measured by pathway length and velocity compared to

CD4 T cells on control peptide-treated LEC (Fig. 6a). Decreased mobility was accompanied by increased binding of CD4 T cells to nciLT but not ciLT or control peptide-treated LEC (Fig. 6b). In contrast, nciLT did not increase the binding of CD4 T cells to LT β R^{-/-} LEC (Fig. 6c), further confirming the role of LT β R in T cell-LEC adhesion.

Since T cells bind endothelial cells through a variety of adhesion molecules, blocking antibodies to several of these receptors^{23,24} were tested for their activity in the binding, migration, and motility assays. Notably, the enhanced binding of CD4 T cells was diminished when the nciLT-treated LEC were pre-incubated with anti-integrin β 4 or anti-VCAM-1, but not a variety of other antibodies (Fig. 6b). Concordantly, CD4 T cell migration across the nciLT-treated LECs, and CD4 T cell motility on nciLT-treated LECs, were restored by these antibodies, but not antibodies to a variety of other integrins (Fig. 6d, e, Supplementary Fig. 4a–c). As noted in Fig. 5e–g, nciLT inhibited migration into lymphatic vessels and the draining LN *in vivo*. Anti-integrin β 4 and anti-VCAM-1 also restored these *in vivo* migration events (Fig. 6f, g). The importance of VCAM-1 for leukocyte TEM across lymphatic endothelium has previously been reported by others and us^{3,25}. Integrin β 4 is involved in endothelial cell integrity²⁶. Unlike other integrin β chains which can bind multiple α chain partners, the β 4 chain only pairs with the α 6 chain, while integrin α 6 also pairs with β 1 (ref. 27). The anti- β 4 mAb used here (346-11A) recognizes the ectodomain of integrin β 4, and has been suggested to dissociate the α 6 β 4 complex²⁷. The anti- α 6 mAb used here (GoH3) inhibits integrin binding to laminin, but has not previously been shown to alter cell migration or motility. The ability of anti- β 4 and the failure of anti- α 6 mAb to alter T-LEC interactions here is likely due to the differences in subunit pairing and in the precise epitope specificity of the mAbs.

To investigate how nciLT altered LEC adhesion receptors and thereby T cell movements, we examined surface expression and distribution. As noted above (Figs. 2a–c, 4a, c–e, Supplementary Fig. 2a), LT β R signaling and nciLT each caused a significant increase in the expression of VCAM-1 on LEC and SVEC4-10 via stimulation of classical NF κ B signaling. Flow cytometric and immunohistochemical analysis of primary LEC *in vitro* and Lyve-1-expressing lymphatic vessels *in vivo* demonstrated the co-expression of integrins α 6 and β 4, but not integrins α E or β 7 (Supplementary Fig. 4d–f). nciLT slightly increased the expression of integrins α 6 and increased β 4 to a much greater degree on LEC *in vitro*. Next, naive CD4 T cells were incubated with primary LEC, unbound T cells washed after 3 h, and the intercellular integrin interactions were examined. Since CD4 T cells did not express integrin β 4, but did express β 7 and α 6 (Supplementary Fig. 4f), the β 4 staining was specific for the LEC. CD4 T cells induced a small increase in integrin β 4 expression along with co-localization of T cells with β 4 expressing LEC under control conditions (Fig. 6h, second row). nciLT again resulted in a marked increase in integrin β 4 expression and markedly more co-localization of the T cells and integrin β 4 on the LEC (Pearson correlation coefficient (PCC): 0.64 ± 0.1), suggesting clustering of the integrin at the T cell-LEC interface (Fig. 6h, third row). This T cell-LEC interaction was inhibited by anti-integrin β 4 mAb (PCC: 0.22 ± 0.1) (Fig. 6h, lower row), commensurate with the binding and motility assays (Fig. 6a–g). Overall, these results demonstrated that LT β R-NIK regulated LEC integrin β 4 and VCAM-1-dependent adhesion, motility, and migration of CD4 T cells by altering the expression and distribution of these molecules.

T lymphocytes activate LEC via the LT α β -LT β R NIK pathway. We recently demonstrated that Treg but not non-Treg use LT α β

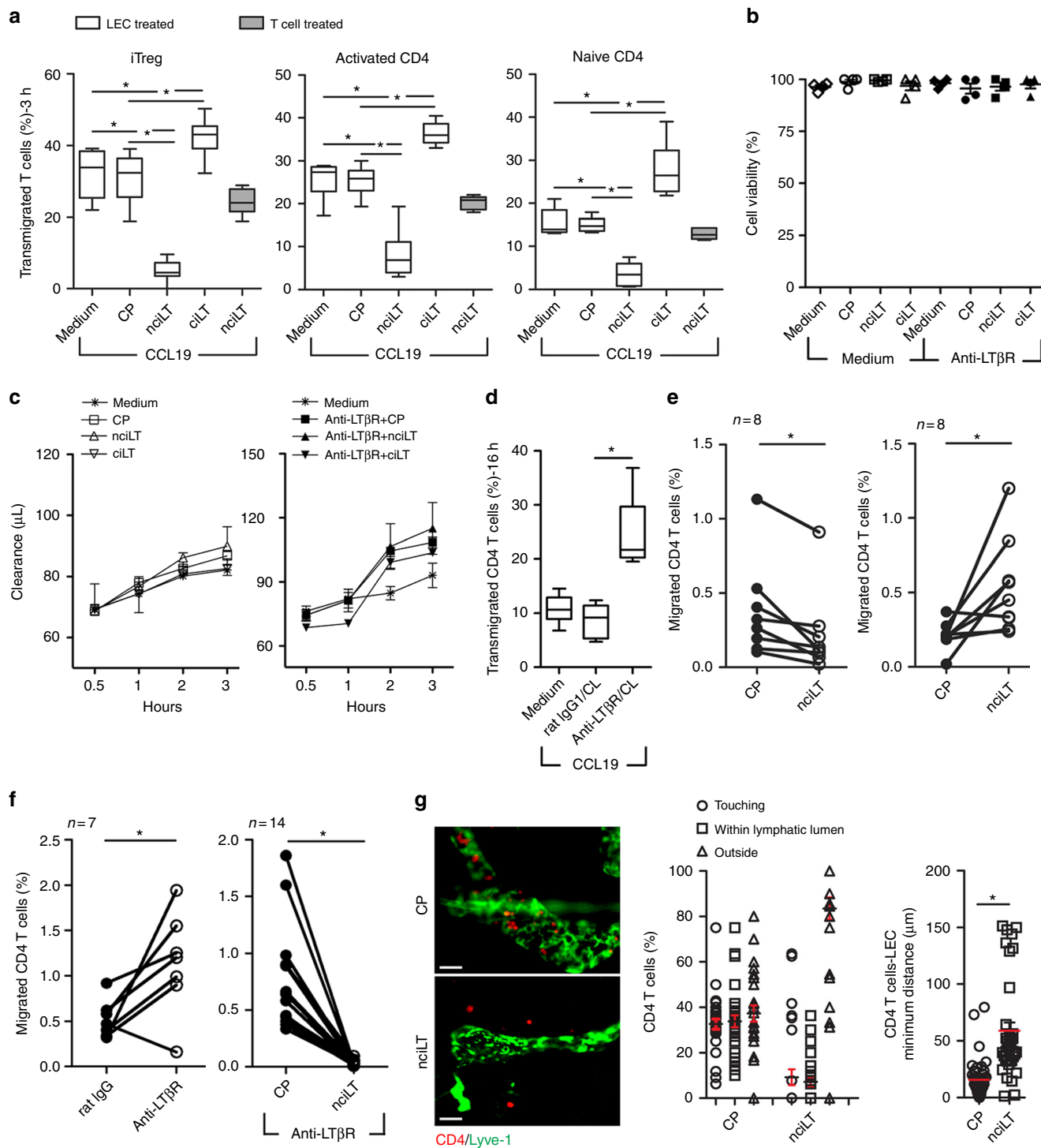
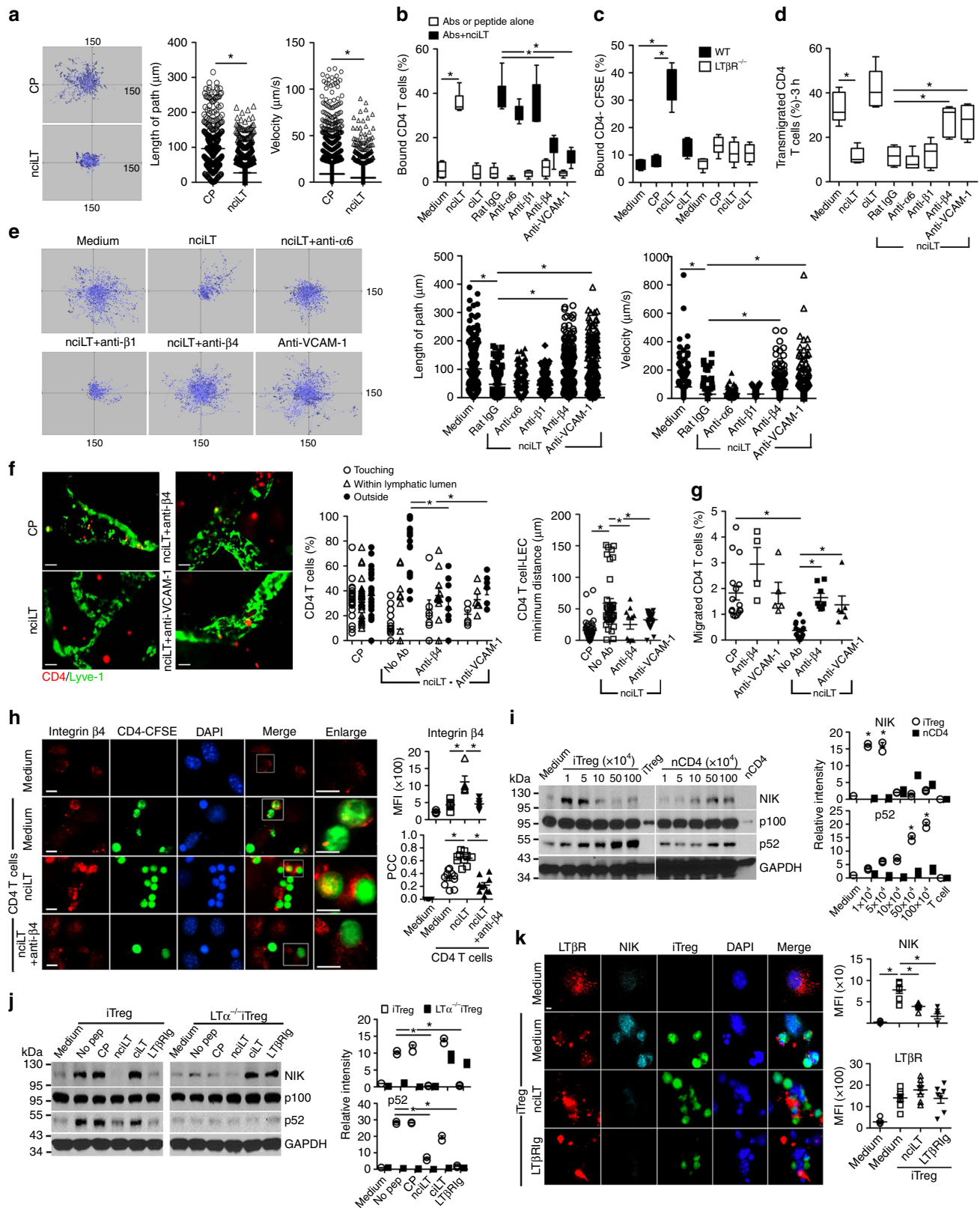


Fig. 5 LTβR peptides that block non-classical NFκB signaling inhibit CD4 T cell migration across LEC. **a** LEC cell layers pretreated with the indicated peptides (20 μM) for 30 min at 37 °C and then Foxp3⁺CD4⁺CD25⁺ iTregs, Foxp3⁻CD25⁻CD4⁺aCD4, or naïve CD4 cells loaded into upper chamber and migrated toward CCL19 (50 ng/mL) for 3 h. **b** LEC incubated with 20 μM nciLT or ciLT peptides for 3 h without or with stimulation with 2 μg/mL anti-LTβR mAb. Cell viability determined by MTT incorporation assay. **c** Time-course monitoring of 0.75% albumin/Evans Blue diffusion across LEC cell layer in Boyden chamber treated as in **b**. **d** LEC cell layers pretreated with anti-LTβR mAb or isotype rat IgG for 30 min at 4 °C, washed and CL with mouse anti-rat IgG1 for 30 min at 37 °C, followed by 16 h incubation, then naïve CD4 cells loaded into the upper chambers and migrated toward CCL19 (50 ng/mL) for 3 h. **e, f** Footpad-popliteal LN migration assay. 1 × 10⁶ CFSE-labelled naïve CD4 T cells mixed with 5 nmol CP (left side), 5 nmol nciLT (right side), or 5 nmol ciLT (right side) without (**e**) or with 1 μg anti-LTβR mAb (**f**), injected into hind footpads. After 16 h popliteal LNs collected and analyzed with flow cytometry. **g** Ear whole-mount staining and migration. CFSE-naïve CD4 T cells injected into ear pinnae pretreated with peptides (5 nmol/ear), and collected after 16 h post injection. Images of T cells and Lyve-1⁺ lymphatic vessels (left). Magnification ×20; scale bar 50 μm. Position (center) and distance (right) of T cells with respect to lymphatic vessels. **a-g** Mean ± SEM of at least three independent experiments. **p* < 0.05 by one-way ANOVA (**a-d**) or by Student's *t*-test (**e-g**)

to engage the $LT\beta R$ -NIK pathway on afferent LEC for TEM to the dLNs³. We further investigated the regulation of the $LT\beta R$ -NIK pathway on LEC and the consequences for T cell migration. Compared to naïve or activated CD4 T cells, iTregs specifically expressed higher levels of cell surface $LT\alpha\beta$ (Supplementary Fig. 5a, b)³. Primary LECs were incubated with various

doses of iTregs or CD4 T cells, and NIK activation was evaluated by immunoblot of LEC lysates after the T cells were removed. Consistent with $LT\beta R$ expression levels, iTreg induced significantly higher levels of NIK activation than naïve or activated CD4 T cells, while $LT\alpha$ -deficient Treg failed to induce NIK activity (Fig. 6i, j, Supplementary Fig. 5c). Moreover, nciLT but



not ciLT suppressed iTreg-induced NIK accumulation and p100 processing, and LT β Rlg also blocked NIK activation (Fig. 6j). Incubation of iTreg with LEC resulted in concentration of LT β R at sites of Treg-LEC contact and the induction of NIK and CCL21, and these events were suppressed by nciLT, while VCAM-1 expression was increased (Fig. 6k, Supplementary Figs. 4c, 5d). In contrast, neither naïve nor activated CD4 T cells induced CCL21, while activated CD4 T cells induced a minor increase in VCAM-1 (Supplementary Figs. 4d, 5e, f). Together, these results demonstrated direct stimulation of LEC LT β R by T cell LT α β , preferential stimulation of the NIK pathway by this interaction, and markedly higher activity from Treg due to higher expression of LT α β .

Targeting LT β R alters contact hypersensitivity. Contact hypersensitivity (CHS) is a T cell-mediated inflammatory response. Hapten sensitization induces migration of dermal DC (dDC) to dLNs for T cell priming^{28,29}. Hapten challenge induces another round of dDC migration from skin to dLNs, stimulation of primed T cells, and recruitment of activated T cells to the site of challenge³⁰. During resolution of inflammation, egress of the inflammatory cells out of the CHS site is required³¹. To test the ability of selective NF- κ B-blocking peptides to also regulate DC migration, we determined that as for T cells, DC TEM in vitro was inhibited by nciLT and enhanced by ciLT (Fig. 7a). nciLT also inhibited skin Langerhans DC migration from skin to dLN in vivo in response to skin painting with FITC (Fig. 7b).

We next assessed the peptides in CHS to provide proof of concept for manipulation of LEC LT β R signaling in an in vivo immunity model. Our results and the literature show that: (1) the peptides specifically affect T cell and DC migration from tissues to draining LN (results here); (2) the LT α β -LT β R interaction does not affect T cell migration from blood to tissues, blood to LN, or LN to efferent lymphatics³; (3) the LT α β -LT β R interaction does not affect T cell viability, proliferation, or apoptosis³ (and results here); (4) for LT α KO and LT β R KO mice there are no changes in migration of T cells to spleen or tissues (note that those mice lack LNs)^{3,6,7}; (5) DC express LT α β ³²⁻³⁴ and LT β R³⁵, which have been implicated in DC homeostasis but not antigen presentation; and (6) the *Drosophila* Antennapedia based peptides, designed to bind and rapidly enter cells, unlike typical peptide antigens^{21,22} are not substantially delivered to draining LNs. The peptides injected in the footpad did not change draining LN architecture, cell distribution, or cell content from 6 to 24 h post injection. Nevertheless, it was possible that the

peptides did not affect residential but rather recirculating leukocyte afferent migration (Supplementary Fig. 53c, d).

To test the in vivo ability of selective NF κ B-blocking peptides to regulate the stages of the CHS response, we administered the peptides at the time of DNFB sensitization (day 0), challenge (day 5, elicitation phase), or 48 h after challenge (day 7, resolution phase) (Fig. 7c). Administration of nciLT to the shaved abdomen by i.d. injection 30 min before sensitization, inhibited CHS 24 h after challenge, with fewer T cells and DC infiltrating the ear compared with controls (Fig. 7di, ei, Supplementary Fig. 6i). Inhibition by nciLT of dDC migration to the dLNs likely may have reduced T cell priming. Additionally, CCL21 production by LEC has a critical role for DC afferent lymphatic migration in CHS^{28,36}, and was suppressed by nciLT (Fig. 4d). Treatment with nciLT or with ciLT in the ear pinna at the time of DNFB challenge and elicitation on day 5 inhibited CHS with reduced T cell infiltration (Fig. 7dii, eii, Supplementary Fig. 6ii). nciLT at this stage may have again interfered with dDC migration to the dLN and stimulation of primed T cells. ciLT may have blocked expression of classical NF κ B-driven inflammatory chemokine (e.g., CCL2) and adhesion molecules (e.g., VCAM-1, ICAM-1) by LEC, which are upregulated and important during CHS³⁷⁻³⁹. ciLT may have also enhanced egress of inflammatory cells out of the ear. By administration of the peptides on day 7, at the start of the resolution stage, nciLT sustained CHS, likely possibly by preventing egress of the inflammatory infiltrate as shown by enhanced T cell and DC infiltration in the ear (Fig. 7eiii). In contrast, ciLT enhanced resolution (Fig. 7diii, Supplementary Fig. 6iii), possibly by inhibiting cytokines and promoting the egress of the inflammatory cells, as fewer CD3 and CD11c cells were present (Fig. 7eiii).

Discussion

Here we found LEC and lymphatic vessels expressed high levels of LT β R which signaled to both classical and non-classical NF κ B pathways^{12,13,40}. NIK, the hallmark of non-classical NF κ B signaling, was constitutively active in resting LEC, and signaling was enhanced by LT β R activation. LT β R NIK stimulation induced RelB nuclear translocation, chemokines such as CCL21 and CXCL12 which promoted T cell or DC migration across LEC, and enhanced T cell TEM migration. LT β R activation also resulted in classical NF κ B signaling, rapid RelA nuclear translocation, and VCAM-1 and CCL2 expression associated with cell migration during inflammation. VCAM-1 expression on LEC or lymphatic vessels was enhanced by the non-classical NF κ B inhibitor nciLT,

Fig. 6 Inhibition of T cell stimulated LT α β -LT β R NIK pathway on LEC enhances T cell binding to LEC through integrin β 4 and VCAM-1. **a** Time-lapse, 2-D microscopy of CD4 T cell migration across LEC. LEC layers in Boyden chambers treated with 20 μ M CP or nciLT for 30 min at 37 $^{\circ}$ C, washed and naïve CD4-CFSE T cell migration to CCL19 (50 ng/mL) monitored for 3 h by live imaging. **b** Binding of naïve CD4 T cells to LEC pretreated with the indicated peptides (20 μ M) with or without anti-integrin mAbs (2 μ g/mL) or anti-VCAM-1 mAb (3 μ g/mL) for 30 min at 37 $^{\circ}$ C. **c** Binding of naïve CD4 T cells to wild type (WT) or LT β R $^{-/-}$ LEC pretreated with the indicated peptides (20 μ M). **d** LEC layers in Boyden chamber treated as in **b**, then naïve CD4 T cells migrated across LEC. **e** LEC layers treated with peptides and mAbs as in **b** for 30 min at 37 $^{\circ}$ C, washed, and naïve CD4 T cell migration toward CCL19 (50 ng/mL) monitored for 3 h of live imaging. **f** Ear whole-mount staining and migration. Pinnae injected with nciLT (5 nmol/ear) with or without anti-integrin β 4 (5 μ g) or anti-VCAM-1 mAbs (15 μ g) 30 min before transfer of naïve CFSE-labeled CD4 T cells (1×10^6 /ear). After 16 h, ears collected and stained for Lyve-1. Images of T cells and Lyve-1 $^{+}$ lymphatic vessels (left). Magnification $\times 20$; scale bar 50 μ m. Position (center) and distance (right) of T cells with respect to lymphatic vessels. **g** Footpad-popliteal LN migration assay. Hind footpads injected with the same doses of peptide or antibodies as in **f**, then 1×10^6 naïve CD4-CFSE T cells transferred. After 16 h, popliteal LN collected and analyzed with flow cytometry. **h** Expression of cell surface integrins on primary LEC. LEC treated with 20 μ M nciLT with or without anti-integrin β 4 mAb (2 μ g/mL) prior to co-culture with 2×10^5 naïve CD4-CFSE for 3 h. Unbound T cells gently washed away before fixation. PCC Pearson's correlation coefficient. Magnification $\times 60$; scale bar 5 μ m. **i, j** Immunoblot of NIK activation in LEC pretreated with the indicated peptides (20 μ M) or LT β Rlg (2 μ g/mL) for 30 min, then incubated with various numbers of purified iTreg or naïve CD4 T cells (**i**) or 5×10^5 wild type or LT α -deficient iTreg (**j**) for 6 h. The bar graphs represent the relative band intensities (mean \pm SEM) from three independent experiments. **k** Expression of LT β R and NIK in primary LEC pretreated with 20 μ M nciLT or 2 mg/mL LT β Rlg for 30 min at 37 $^{\circ}$ C, and co-cultured with 2×10^5 iTreg-CFSE for 6 h. Magnification $\times 60$; scale bar 5 μ m. * $p < 0.05$ by Students' *t*-test (**a**) or by one-way ANOVA (**b-k**)

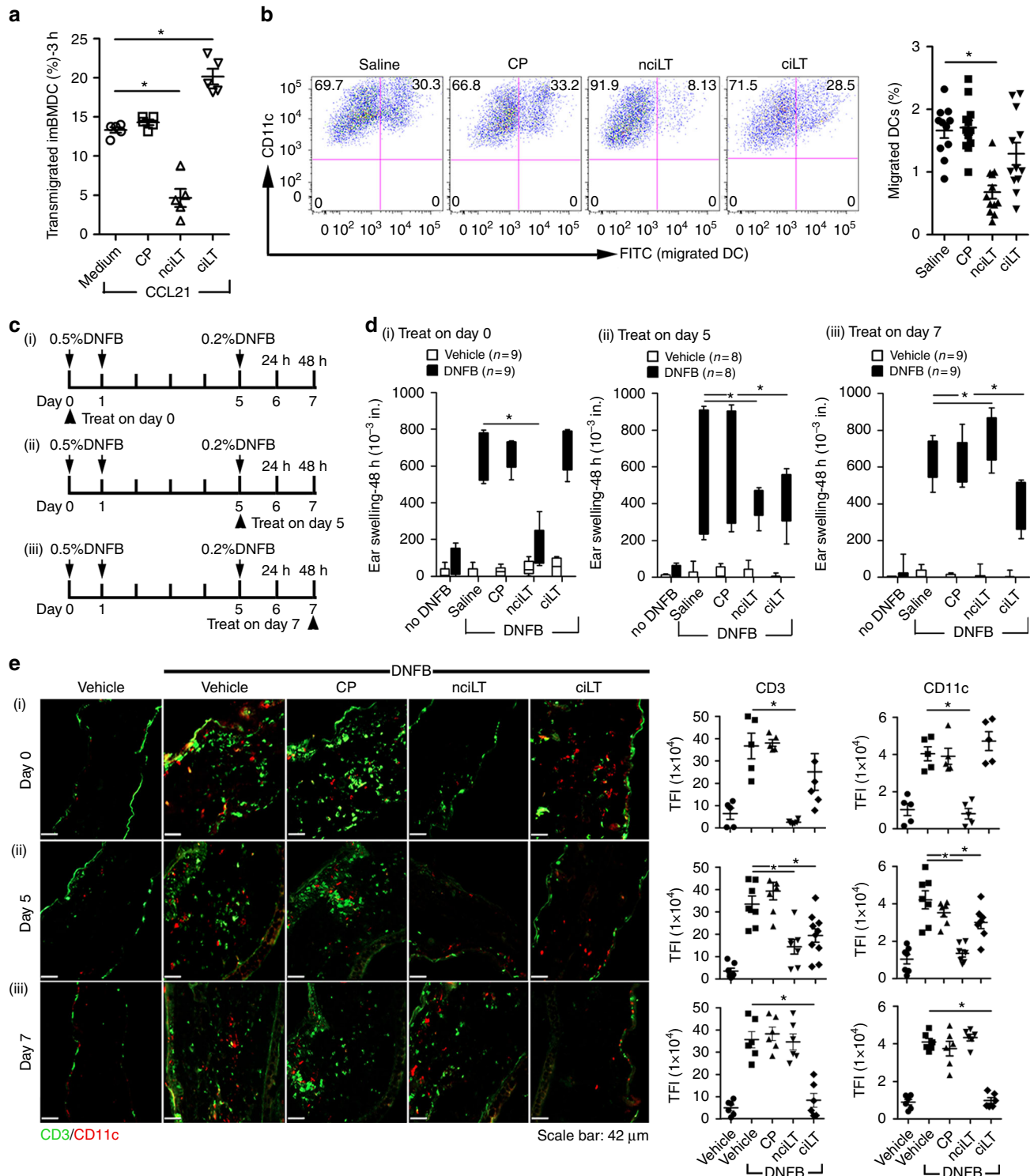


Fig. 7 Inhibition of LTβR signaling alters CHS and leukocyte migration. **a** In vitro DC migration to CCL21 (50 ng/ml) through LEC treated with the indicated peptides (20 μM). **b** In vivo DC migration assay. i.d. injection of the indicated peptides (20 nmol) to the shaved abdomen, followed 30 min later by FITC painting. After 16 h, inguinal and axillary LNs collected and analyzed with flow cytometry. **c** Experimental design schematic. 20 nmol of indicated peptides injected i.d. in the abdomen (100 μL, day 0) or 10 nmol in each ear (30 μL, day 5 or day 7) 30 min before DNFB painting on days 0 or 5. **d, e** CHS analyzed by ear swelling measured 48 h after DNFB challenge (**d**), or immunohistochemistry for CD11c⁺ DC and CD3⁺ T cells (**e**). Magnification ×20; scale bar 42 μm. TFI total fluorescence intensity. Representative of three independent experiments with 3 mice/group. *p < 0.05 by one-way ANOVA

which caused firm adhesion of T cells on LEC, further showing that non-classical and classical NFκB signaling interacted to regulated LEC function. In contrast, the classical NFκB-blocking peptide ciLT enhanced CCL21 production in LEC and promoted T cell migration. Molecular interactions indicated upstream

crosstalk between the two arms of LTβR–NFκB pathways, such that nciLT or ciLT decoy peptides influenced TRAF3 or TRAF2 recruitment to the receptor. Together these data demonstrated major roles for LTβR related NFκB pathways in regulating LEC function and TEM.

TRAFs play distinct functional roles for different receptors and cell types. Differential recruitment of TRAF2 and TRAF3 to the LT β R contributes to distinct signaling functions^{18,41}. Our results suggested that in primary resting LEC, TRAF3 constitutively bound LT β R resulting in basal low level NIK activity (Supplementary Fig. 7ai). TRAF3 does not directly ubiquitinate NIK, but rather bridges the TRAF2-cIAP1/2 complex to NIK, leading to rapid turnover of NIK in resting cells^{41,42}. Thus, the preferential binding of TRAF3 instead of TRAF2 to the receptor may favor constitutive NIK activation. Inhibition of cIAP1/2 resulted in an increase in NIK and p100, confirming the direct involvement of cIAP1/2 in NIK decay. After receptor activation, TRAF2 was recruited to the receptor complex, in which cIAP1/2 ubiquitinates and degrades TRAF2 and TRAF3 (Supplementary Fig. 7aii). Once TRAF2 and TRAF3 are degraded, NIK is released from the complex and stabilized from degradation by cIAP1/2. Sequestration of TRAF3 from the receptor complex by the decoy receptor nciLT targeted TRAFs and NIK for ubiquitination by cIAP1/2, thereby inhibiting NIK activity (Supplementary Fig. 7aiii).

Our results showed LT β R-NF κ B/RelA activation without I κ B-degradation (Supplementary Fig. 7ai). Since TRAF2 and TRAF3 have been shown to be mediators⁴³ or inhibitors^{11,44} of NF κ B activation, respectively, the data implicate TRAF3 suppression of NF κ B activity as predominant in resting LEC. TRAF3 may also suppress the recruitment of TRAF2 to the activated LT β R and prevent TRAF2-mediated classical NF κ B signaling (Supplementary Fig. 7bii). Blockade of TRAF2 recruitment to LT β R by the cILT decoy peptide also blocked TRAF3 binding to LT β R, prevented further TRAF2 and TRAF3 degradation induced by receptor activation (Supplementary Fig. 7biii), but did not affect LT β R-NIK activation. Overall, the results supported a model where TRAF2 was the mediator of classical NF κ B signaling in LEC, and TRAF3 was the critical component for the LT β R-non-classical NF κ B axis in LEC.

LT α 1 β 2 is mainly expressed on activated lymphocytes and mature DCs^{18,32–34,40}. LT β R is widely expressed on non-lymphoid endothelial cells including LEC and BEC, intestinal epithelial cells, and LN stromal cells⁴⁰. The distribution of receptors and ligands suggests that the LT α 1 β 2–LT β R axis serves as a bridge for immune cell trafficking between lymphoid and non-lymphoid tissues. NIK signaling primarily regulates this bridge as shown by blocking the signaling with nciLT, which suppressed CCL21 and CXCL12 production and prevented T cell and DC migration across LEC or lymphatic vessels. By expressing high levels of LT α 1 β 2, Treg preferentially and directly engaged LT β R-NIK signaling, compared to other CD4 T cells or DC. The Treg–LEC interaction resulted in enhanced TEM across LEC and triggered VCAM-1 and CCL21 expression by LEC. These data confirmed our previous report that LT signaling was particularly important for suppressive regulatory cell migration and LEC homeostasis³. Non-Treg CD4 T cells and DC, which expressed lower levels of LT α 1 β 2, did not stimulate LEC LT β R but did require the constitutive LEC NIK activation for TEM. Presumably these CD4 T cells and DC migrate toward and across LEC via CCR7–CCL21 (ref.⁴⁵). The differential use of the LT α 1 β 2–LT β R axis by Treg versus non-Treg cells suggest that Treg may modify the migration of these other cells by modulating LEC responses. Our data show that nciLT inhibited naïve and activated T cell migration in vitro (Fig. 5a), and that nciLT inhibited naïve T cell migration in vivo (Figs. 5e, 6g). However, since it is generally considered that naïve T cells migrate via blood to LN, while activated and memory T cell migrate via tissues and lymph to LN⁴⁶, future investigations should determine how the LT system regulates the migration of activated and memory CD4 and CD8 cells in vivo.

In vivo targeting of T cell and DC migration by the LT β R blocking peptides in CHS showed that these peptides and signaling pathways are relevant for disease; that individual kinetic components of immune responses, such as sensitization, elicitation, and resolution, can be precisely targeted; and that both lymphocytes and myeloid cells are equally influenced by these pathways. These findings open up the possibility for other applications and investigations of how lymphatic signaling and trafficking regulate immunity. These peptides may serve as a foundation for compound screening and drug discovery for novel therapeutics to regulate immune responses.

Methods

Mice. C57BL/6 (WT, LT β R^{-/-}, Lta^{-/-}) (7–10 weeks) were purchased from The Jackson Laboratory (Bar Harbor, ME). Prox1-Cre-ER^{T2} mice were from Guillermo Oliver (St. Jude's Hospital, Memphis, TN)⁴⁷, and LT β R^{fl/fl} were from Thomas Hehlhans (University of Regensburg, Regensburg, Germany)⁴⁸. For conditional depletion of LT β R in Prox1-expressing LEC and lymphatic vessels, Prox1-Cre-ER^{T2}–LT β R^{fl/fl} (KO) and littermate control Prox1-Cre-ER^{T2}–LT β R^{fl/fl} (WT) mice were injected i.p. with tamoxifen (Sigma-Aldrich, St. Louis, MO) 0.125 mg/g i.p. suspended in corn oil for 5 consecutive days, followed by a chase period of 10 days. Foxp3GFP mice on a C57BL/6 background were from Dr. A. Rudensky (Memorial Sloan Kettering Cancer Center)⁴⁹. All animal experiments were performed in accordance with Institutional Animal Care and Use Committee approved protocols.

Cells. C57BL/6 mouse primary dermal LECs (C57-6064 L) were from Cell Biologics, Inc. (Chicago, IL), and were cultured according to the manufacturer's instructions in manufacturer-provided mouse endothelial cell medium supplemented with 5% fetal bovine serum (FBS), 2 mM L-glutamine, 100 IU/mL penicillin, vascular endothelial growth factor, endothelial cell growth supplement, heparin, epidermal growth factor, and hydrocortisone. SVEC4-10 (CRL-2181) cells were from American Type Culture Collection, and were cultured in Dulbecco's modified Eagle's medium (DMEM) with 4.5 g/L glucose, containing 10% (v/v) FBS, 2 mM L-glutamine, 100 IU/mL penicillin, and 100 μ g/mL streptomycin.

Peptide synthesis and reconstitution. Peptides were synthesized by GenScript. All peptides were >95% purity, dissolved in endotoxin-free ultrapure water, and concentrations quantified by spectrophotometry⁵⁰ after reconstitution and stored at –80 °C.

CD4⁺ T cells and bone marrow derived dendritic cell. CD4⁺ T cells from mouse LNs and spleens were isolated using CD4⁺-negative selection (Stemcell Technologies, Cambridge, MA), and were cultured as previously described (1). Briefly CD4⁺CD25⁻Foxp3GFP⁻ WT or Lta^{-/-} cells with >98% purity were sorted using a FACS Aria II (BD Biosciences). The sorted GFP⁻ naïve CD4 T cells (nCD4) (5 \times 10⁴) were then co-cultured with T cell-depleted, 800 rad-irradiated C57BL/6 splenocytes as stimulator cells (5 \times 10⁴) in U-bottom 96-well plates for 5 days at 37 °C in 5% CO₂, with IL-2 (20 ng/mL; eBioscience, San Diego, CA), anti-CD3 ϵ mAb (1 μ g/mL, clone 145-2C11; eBioscience) for activated T cells (aCD4); and human TGF- β 1 (10 ng/mL; eBioscience) for induced regulatory T cells (iTreg). Cells were cultured in RPMI 1640 supplemented with 10% FBS, 1 mM sodium pyruvate, 2 mM L-glutamine, 100 IU/mL penicillin, 100 μ g/mL streptomycin, non-essential amino acids and 2 \times 10⁻⁵ M 2-ME (Sigma-Aldrich). BMDCs were generated as described⁵¹. Briefly, bone marrow (BM) cells of wild-type mice were treated with 10 ng/mL GM-CSF (R&D Systems, Minneapolis, MN) for 10 days in Petri dishes, and the loosely attached cells were collected and CD11c⁺ DC were purified by CD11c-positive selection kit (Stemcell Technologies).

Primary murine skin LEC purification and culture. Abdominal skin and ears from 5- to 6-week-old wild type and LT β R^{-/-} C57BL/6 mice were collected and digested in 4 mg/mL collagenase D (Roche, Indianapolis, IN) at 37 °C for 1 h. The dissociated cells were washed, depleted of CD45⁺ cells using MojoSort Mouse CD45 Nanobeads (Biolegend, Inc, San Diego, CA), re-suspended in mouse endothelial cell medium (Cell Biologics, Inc), and plated in six-well tissue culture plates for 3–5 days until the adherent cells reached confluency. The cells were dissociated with 0.25% trypsin-EDTA (Thermo Fisher, Waltham, MA) and the LEC were purified with Lyve-1-FITC (eBioscience) using anti-FITC positive selection kit (Stemcell Technologies).

Flow cytometry. LECs in phosphate-buffered saline (PBS) containing 0.2 mM calcium, 0.1 mM magnesium, and 0.5% w/v bovine serum albumin (BSA) were treated with anti-CD16/32 (clone 93; eBioscience) to block Fc receptors, and then stained with antibodies to cell surface molecules in the same buffer. Flow cytometry antibody used was: APC-eFlour780-anti-mouse CD4 (GK1.5; eBioscience); PE-anti-mouse CD25 (PC61.5; eBioscience); PE-anti-mouse CD44 (IM7; eBioscience);

APC-anti-mouse VCAM-1 (clone 647; eBioscience). For detection of LT α 2 β 1, T cells were incubated with MOPC21 or LT β Rig at 2 μ g/mL for 60 min at 37 °C in HBSS with 2% FBS. Cells were washed, and then stained for 45 min at 4 °C with BV421-rat anti-mouse IgG1 along with antibodies to other cell surface markers. Cells were then washed and fixed with 4% paraformaldehyde and run on an LSR Fortessa flow cytometer (BD Biosciences, San Jose, CA). Results were analyzed with FlowJo 8.7 (Treestar). Flow cytometry gating information is included in Supplementary Fig. 8.

MTT viability assay. LECs were plated into 24-well tissue culture plates, incubated overnight, and treated with 20 μ M peptides with or without agonist anti-LT β R (2 μ g/mL) for 3 h. The cells were washed and followed by 3-h incubation with 0.5 mg/mL MTT (3-(4, 5-dimethylthiazol-2-yl)-2,5 diphenyl tetrazolium bromide) (Sigma-Aldrich). Fifty microliters DMSO was added to cells before reading OD at 540 nm.

Evans Blue endothelial permeability assay. 2.5×10^5 primary LEC or SVEC4-10 were plated on inverted 0.2% (w/v) gelatin-coated Boyden chamber transwell polycarbonate membranes. The cell layers were treated with various conditions as noted in the text and figure legends prior to adding with 100 μ L of 0.67 mg/mL Evans Blue (Sigma-Aldrich) diluted in IMDM migration medium containing fat-free BSA (40 mg/mL) (Gemini Bio-Products, Broderick, CA). Six hundred microliters fresh migration medium without phenol red was added to the lower chamber. After 0.5, 1, 2, and 3 h, lower chamber medium was collected into flat-bottom 96-well tissue culture (TC) plate, and the optical density at 650 nm was measured in a microplate reader (TECAN, San Jose, CA).

T cell-LEC binding assay. 2×10^4 primary LECs or SVEC4-10 were plated on 0.2% (w/v) gelatin-coated flat-bottom 96-well TC plate. The LEC layers were treated with peptides or antibodies as noted in the text and figure legends before adding with 2×10^5 CFSE-labelled CD4 T cells in IMDM migration buffer without a phenol red indicator. After 3 h at 37 °C in 5% CO₂, non-bound cells were removed by gently washing and replacing with PBS containing 0.1 mM MgCl₂ and CaCl₂. Control wells with input CFSE-CD4 T cells remain unwashed. The fluorescein intensity (FI) from the bound CFSE-CD4 T cells in the plate was measured with a microplate reader. Percentage of bound CFSE-CD4 T cells were calculated as $100 \times (\text{FI of sample} - \text{FI of plate/cell background}) / \text{FI of input CFSE-CD4 T cells}$.

Real-time PCR. One microgram of total RNA extracted using Trizol reagent (Invitrogen) was reverse-transcribed into cDNA with GoScript™ Reverse Transcription System (Promega, Fitchburg, WI). mRNA expression levels were quantified by real-time PCR using SYBR Green Master Mix with an ABI Prism 7900HT (Applied Biosystems, Foster City, CA). Values for specific gene expression were normalized to house-keeping HPRT gene expression, and were calculated as: $2^{-(\text{Ct of HPRT} - \text{Ct of specific gene})}$. Sequences of the primer used were: mVCAM-1 forward 5'-GCGAGGATGCCGGCATATACG-3', mVCAM-1 reverse 5'-TGCGCAGTAGAGTGCAA GG A-3'; mCCL2 forward 5'-TCCACTACCTTTCCACAAC C-3'; mCCL2 Reverse: 5'-GGATCCACACCTTGCAITTTAA-3'; mCXCL12 forward 5'-CTCTGCATCAGTGACGGTAA-3', mCXCL12 reverse 5'-CTTCAGC CGTGCAACAATCT-3'; CCL21 forward 5'-AAGGCAGTGATGGAGGGG-3' and CCL21 reverse 5'-CGGTAAGAACAGGATTG-3'.

ELISA. 5×10^5 LECs or SVEC4-10 cells were plated in 12-well plates and treated with 20 μ M peptides for 30 min at 37 °C. Cells were then washed and incubated with anti-LT β R agonistic mAb (2 μ g/mL) for 30 min at 4 °C, followed by washing and then crosslinking with anti-rat IgG (2 μ g/mL) for 6 or 16 h at 37 °C. The supernatants were collected and stored in -80 °C. Mouse CCL2 and CCL21 were measured with ELISA kits from Biologend, Inc. and R&D Systems, respectively.

Immunoblotting and co-immunoprecipitation. LECs were lysed in buffer containing 20 mM Hepes (pH 7.4), 150 mM NaCl, 10 mM NaF, 2 mM Na₃VO₄, 1 mM EDTA, 1 mM EGTA, 0.5% Triton X-100, 0.1 mM DTT, 1 mM PMSF and protease inhibitor cocktail (Roche). Protein in the cell extract was quantified using protein quantification kit (Bio-Rad, Philadelphia, PA) and 10 μ g total protein was run on Novex™ WedgeWell™ 4–20% Tris-Glycine Mini Gels (Invitrogen) and transferred to an Immobilon-P membrane (Bio-Rad). Membranes were probed with anti-p100/p52, NIK, phospho-IKK α / β (Ser176/180) (16A6), I κ B α , TRAF2, TRAF3, and GAPDH antibodies. For co-IP assays, 500 μ g total protein of cell extract was incubated with 1 μ g of anti-mLT β R (5G11b) overnight, followed by 4 h incubation with 25 μ L protein G Agarose beads (Sigma-Aldrich). The beads were then washed with lysis buffer and boiled in 2 \times Laemmli sample buffer (Bio-Rad). Uncropped immunoblotting images are included in Supplementary Fig. 9.

Transendothelial migration. Transmigrations across endothelial cells were described previously³. Briefly the inverted transwell insert (24-well; Corning International) with 5 μ m pore size was coated with 0.2% (w/v) gelatin (Bio-Rad) for 1 h at 37 °C before loading with 1.5×10^5 primary skin LEC or SVEC4-10 in 100 μ L mLEC or cDMEM medium. After 2 days, the LEC cell layers were treated with

various conditions as noted in the text and figure legends prior to adding 2×10^5 T cells or DCs in 100 μ L to the upper chamber of transwell plate while the lower chamber contained mCCL19 or CCL21 (50 ng/mL; R&D systems). All cells or reagents were prepared in IMDM containing transferrin and 0.5% (w/v) fatty acid-free BSA (Gemini). T cells that migrated to the lower chamber after 3 h at 37 °C were counted.

Time-lapse microscopy. Purified naive CD4 T cells were incubated with 5 μ M CFSE at 37 °C for 5 min, quenched with 50% FBS at 4 °C for 5 min and were washed in migration buffer. CFSE-labelled CD4 T cells (5×10^4 cells per transwell) migrating across endothelial monolayers to CCL19 (50 ng/mL) were visualized by EVOS FL Auto Cell Imaging System (Thermo Fisher Scientific) with a $\times 20$ objective. One image was captured every 5 min for 3 h. Cell tracks were analyzed with Velocity version 6.3 software (Perkin Elmer).

Immunohistochemistry. LEC monolayers were stained for surface VCAM-1, LT β R, or Lyve-1 with rat anti-mouse VCAM-1 (Clone 429; eBioscience), rat anti-mouse LT β R (Clone 3C8; eBioscience), or rabbit-anti-mouse Lyve-1 (70R-LR003, Fitzgerald, Acton, MA), and then were fixed for 20 min at 4 °C with 4% (w/v) paraformaldehyde (Affymetrix). Cells were permeabilized with PBS 0.2% (v/v) Triton X-100 (Sigma-Aldrich), and treated with 4% donkey serum for 30 min then incubated with rabbit-anti-mouse CXCL12 (eBioscience), goat-anti-mouse CCL21 (Clone AF457; R&D System), anti-NIK mouse monoclonal antibody (Clone A-12; Santa Cruz Biotechnology), or rabbit-anti-mouse RelA (Cell Signaling) or RelB (Thermo Fisher Scientific) for nuclear translocation staining overnight at 4 °C. The primary antibodies were detected with Alexa Fluor 448, 647 (Cy5), or 546 (Cy3)-conjugated donkey anti-goat, donkey anti-rabbit, or donkey anti-rat secondary antibodies (Jackson ImmunoResearch, West Grove, PA) for 1 h at 4 °C. Transwell membranes were transferred onto glass slides and visualized by fluorescent microscopy (Zeiss LSM 510 Meta and LSM5 Duo) with a $\times 60$ or $\times 20$ objective. Images were analyzed with Velocity version 6.3 software. For specific molecules, the fluorescence intensity was measured as mean fluorescence intensity over the entire field. For specific cells, the total number of cells stained with specific fluorescence was measured as total fluorescence intensity. Pearson's correlation coefficient (PCC) was used to quantify the degree of co-localization between fluorophores.

Footpad and whole-mount ear migration assays. Mice were anesthetized and 1×10^6 CD25⁺ Tregs or CD4⁺ non-Tregs were injected intradermally into the footpads or ear pinnae in 20 μ L PBS as we previously described. For footpad assays, draining popliteal LN were collected 12 h post paired injection (control vs ncILT or ciLT treatments) both footpads in each mouse and processed for flow cytometry. For ear pinnae assays, whole-mount ears were collected 4–16 h post injection, fixed for 10 min at room temperature with 4% paraformaldehyde, then stained with anti-Lyve-1 at 5 μ g/mL (70R-LR003, Fitzgerald), anti-CCL21 (AF457, R&D Systems) at 5 μ g/mL in PBS, 0.5% BSA, and 0.3% Triton X-100 overnight at 4 °C; washed with PBS, 0.5% BSA, and 0.3% Triton X-100; stained with 5 μ g/mL donkey anti-rabbit Alexa Fluor 488 and donkey anti-goat Cy3 (Jackson ImmunoResearch) for 2 h at 4 °C, washed twice in PBS, 0.5% BSA, and 0.3% Triton X-100; fixed once more as above, transferred to glass slides, and mounted with Prolong Gold (Life Technologies, Carlsbad, CA). Distance of T cells from lymphatic vessels calculated with minimum distance program in Velocity 6.3.

CHS and FITC painting. Twenty-five microliters of 0.5% (v/v) DNFB in acetone/olive oil (4:1) solution was applied onto the shaved abdomen of the mice on days 0 and 1 (sensitization phase). On day 5, the right ear was treated with 20 μ L 0.2% DNFB (10 μ L on each side of the pinna), and the same for the left ear with 20 μ L acetone/olive oil (challenge phase). Ear swelling was measured with a digimatic thickness gauge (Mitsutoyo, Kanagawa-ken, Japan) before and after 24 to 48 h DNFB challenge. The CHS response (ear swelling) was calculated by subtracting pre-challenge ear thickness for each animal. After euthanasia at the indicated days, the ears were removed and fixed with 10% formaldehyde in PBS and embedded in paraffin for hematoxylin and eosin staining, or were unfixed and embedded in OTC compound (Sakura Finetek, Torrance, CA), and processed for immunohistochemistry staining. In vivo DC migration was performed on shaved abdomen as described⁵². Briefly, fluorescein isothiocyanate (FITC, Sigma) 4 mg/mL was dissolved in 1:1 acetone:dibutyl phthalate (Sigma) and 50 μ L applied to the abdominal skin. Recovered inguinal and axillary LNs were digested in 2 mg/mL collagenase D (Roche) for 30 min at 37 °C. Cells were then passed through a 100 μ m cell strainer, and stained for flow cytometry.

Statistical analysis. Numerical data are presented as mean \pm SEM. Significance differences was evaluated using one-way ANOVA and Prism 5 software. Asterisks mark data statistically different from the controls, with *p*-values noted in the figure legends. A *p* value of <0.05 was considered significant for one-way ANOVA and Student *t*-tests. The number of replicates is noted in the figure legends.

Data availability. The authors declare that [the/all other] data supporting the findings of this study are available within the paper and its supplementary information files.

Received: 3 November 2017 Accepted: 2 June 2018

Published online: 01 August 2018

References

- Butcher, E. C. & Picker, L. J. Lymphocyte homing and homeostasis. *Science* **272**, 60–66 (1996).
- Schwab, S. R. & Cyster, J. G. Finding a way out: lymphocyte egress from lymphoid organs. *Nat. Immunol.* **8**, 1295–1301 (2007).
- Brinkman, C. C. et al. Treg engage lymphotoxin beta receptor for afferent lymphatic transendothelial migration. *Nat. Commun.* **7**, 12021 (2016).
- Zhang, N. et al. Regulatory T cells sequentially migrate from inflamed tissues to draining lymph nodes to suppress the alloimmune response. *Immunity* **30**, 458–469 (2009).
- Xiong, Y., Ahmad, S., Iwami, D., Brinkman, C. C. & Bromberg, J. S. T-bet regulates natural regulatory T cell afferent lymphatic migration and suppressive function. *J. Immunol.* **196**, 2526–2540 (2016).
- Rennert, P. D., Browning, J. L., Mebius, R., Mackay, F. & Hochman, P. S. Surface lymphotoxin alpha/beta complex is required for the development of peripheral lymphoid organs. *J. Exp. Med.* **184**, 1999–2006 (1996).
- De Togni, P. et al. Abnormal development of peripheral lymphoid organs in mice deficient in lymphotoxin. *Science* **264**, 703–707 (1994).
- Beinke, S. & Ley, S. C. Functions of NF-kappaB1 and NF-kappaB2 in immune cell biology. *Biochem. J.* **382**, 393–409 (2004).
- Hostager, B. S. & Bishop, G. A. Cutting edge: contrasting roles of TNF receptor-associated factor 2 (TRAF2) and TRAF3 in CD40-activated B lymphocyte differentiation. *J. Immunol.* **162**, 6307–6311 (1999).
- Xu, L. G. & Shu, H. B. TNFR-associated factor-3 is associated with BAFF-R and negatively regulates BAFF-R-mediated NF-kappa B activation and IL-10 production. *J. Immunol.* **169**, 6883–6889 (2002).
- Bista, P. et al. TRAF3 controls activation of the canonical and alternative NFkappaB by the lymphotoxin beta receptor. *J. Biol. Chem.* **285**, 12971–12978 (2010).
- Dejardin, E. et al. The lymphotoxin-beta receptor induces different patterns of gene expression via two NF-kappaB pathways. *Immunity* **17**, 525–535 (2002).
- Madge, L. A., Kluger, M. S., Orange, J. S. & May, M. J. Lymphotoxin-alpha 1 beta 2 and LIGHT induce classical and noncanonical NF-kappa B-dependent proinflammatory gene expression in vascular endothelial cells. *J. Immunol.* **180**, 3467–3477 (2008).
- Basak, S. et al. A fourth IkappaB protein within the NF-kappaB signaling module. *Cell* **128**, 369–381 (2007).
- Mackay, F. et al. Both the lymphotoxin and tumor necrosis factor pathways are involved in experimental murine models of colitis. *Gastroenterology* **115**, 1464–1475 (1998).
- Fava, R. A. et al. A role for the lymphotoxin/LIGHT axis in the pathogenesis of murine collagen-induced arthritis. *J. Immunol.* **171**, 115–126 (2003).
- Chiang, E. Y. et al. Targeted depletion of lymphotoxin-alpha-expressing TH1 and TH17 cells inhibits autoimmune disease. *Nat. Med.* **15**, 766–773 (2009).
- Ganef, C. et al. Induction of the alternative NF-kappaB pathway by lymphotoxin alphabeta (LTalphabeta) relies on internalization of LTbeta receptor. *Mol. Cell Biol.* **31**, 4319–4334 (2011).
- Force, W. R. et al. Discrete signaling regions in the lymphotoxin-beta receptor for tumor necrosis factor receptor-associated factor binding, subcellular localization, and activation of cell death and NF-kappaB pathways. *J. Biol. Chem.* **275**, 11121–11129 (2000).
- Ye, H., Park, Y. C., Kreishman, M., Kieff, E. & Wu, H. The structural basis for the recognition of diverse receptor sequences by TRAF2. *Mol. Cell* **4**, 321–330 (1999).
- Piao, W. et al. A decoy peptide that disrupts TIRAP recruitment to TLRs is protective in a murine model of influenza. *Cell Rep.* **11**, 1941–1952 (2015).
- Piao, W. et al. Recruitment of TLR adapter TRIF to TLR4 signaling complex is mediated by the second helical region of TRIF TIR domain. *Proc. Natl Acad. Sci. USA* **110**, 19036–19041 (2013).
- Berlin, C. et al. Alpha 4 beta 7 integrin mediates lymphocyte binding to the mucosal vascular addressin MadCAM-1. *Cell* **74**, 185–195 (1993).
- DeNucci, C. C., Pagan, A. J., Mitchell, J. S. & Shimizu, Y. Control of alpha4beta7 integrin expression and CD4 T cell homing by the beta1 integrin subunit. *J. Immunol.* **184**, 2458–2467 (2010).
- Johnson, L. A. et al. An inflammation-induced mechanism for leukocyte transmigration across lymphatic vessel endothelium. *J. Exp. Med.* **203**, 2763–2777 (2006).
- Niessen, C. M. et al. Deficiency of the integrin beta 4 subunit in junctional epidermolysis bullosa with pyloric atresia: consequences for hemidesmosome formation and adhesion properties. *J. Cell Sci.* **109**(Pt 7), 1695–1706 (1996).
- Sonnenberg, A., Linders, C. J., Daams, J. H. & Kennel, S. J. The alpha 6 beta 1 (VLA-6) and alpha 6 beta 4 protein complexes: tissue distribution and biochemical properties. *J. Cell Sci.* **96**(Pt 2), 207–217 (1990).
- Engeman, T. M., Gorbachev, A. V., Gladue, R. P., Heeger, P. S. & Fairchild, R. L. Inhibition of functional T cell priming and contact hypersensitivity responses by treatment with anti-secondary lymphoid chemokine antibody during hapten sensitization. *J. Immunol.* **164**, 5207–5214 (2000).
- Fukunaga, A., Khaskhely, N. M., Sreevidya, C. S., Byrne, S. N. & Ullrich, S. E. Dermal dendritic cells, and not Langerhans cells, play an essential role in inducing an immune response. *J. Immunol.* **180**, 3057–3064 (2008).
- Piguot, P. F., Graue, G. E., Hauser, C. & Vassalli, P. Tumor necrosis factor is a critical mediator in hapten induced irritant and contact hypersensitivity reactions. *J. Exp. Med.* **173**, 673–679 (1991).
- Ortega-Gomez, A., Perretti, M. & Soehnlein, O. Resolution of inflammation: an integrated view. *EMBO Mol. Med.* **5**, 661–674 (2013).
- Moussin, C. & Girard, J. P. Dendritic cells control lymphocyte entry to lymph nodes through high endothelial venules. *Nature* **479**, 542–546 (2011).
- Kumar, V. et al. A dendritic-cell-stromal axis maintains immune responses in lymph nodes. *Immunity* **42**, 719–730 (2015).
- Upadhyay, V. & Fu, Y. X. Lymphotoxin signalling in immune homeostasis and the control of microorganisms. *Nat. Rev. Immunol.* **13**, 270–279 (2013).
- Kabashima, K. et al. Intrinsic lymphotoxin-beta receptor requirement for homeostasis of lymphoid tissue dendritic cells. *Immunity* **22**, 439–450 (2005).
- Russo, E. et al. Intralymphatic CCL21 promotes tissue egress of dendritic cells through afferent lymphatic vessels. *Cell Rep.* **14**, 1723–1734 (2016).
- Vigl, B. et al. Tissue inflammation modulates gene expression of lymphatic endothelial cells and dendritic cell migration in a stimulus-dependent manner. *Blood* **118**, 205–215 (2011).
- Ishimoto, T. et al. Downregulation of monocyte chemoattractant protein-1 involving short interfering RNA attenuates hapten-induced contact hypersensitivity. *Mol. Ther.* **16**, 387–395 (2008).
- Teijeira, A. et al. T cell migration from inflamed skin to draining lymph nodes requires intralymphatic crawling supported by ICAM-1/LFA-1 interactions. *Cell Rep.* **18**, 857–865 (2017).
- Schneider, K., Potter, K. G. & Ware, C. F. Lymphotoxin and LIGHT signaling pathways and target genes. *Immunol. Rev.* **202**, 49–66 (2004).
- Vallabhapurapu, S. et al. Nonredundant and complementary functions of TRAF2 and TRAF3 in a ubiquitination cascade that activates NIK-dependent alternative NF-kappaB signaling. *Nat. Immunol.* **9**, 1364–1370 (2008).
- Liao, G., Zhang, M., Harhaj, E. W. & Sun, S. C. Regulation of the NF-kappaB-inducing kinase by tumor necrosis factor receptor-associated factor 3-induced degradation. *J. Biol. Chem.* **279**, 26243–26250 (2004).
- Kim, Y. S., Nedospasov, S. A. & Liu, Z. G. TRAF2 plays a key, nonredundant role in LIGHT-lymphotoxin beta receptor signaling. *Mol. Cell Biol.* **25**, 2130–2137 (2005).
- He, J. Q., Saha, S. K., Kang, J. R., Zarnegar, B. & Cheng, G. Specificity of TRAF3 in its negative regulation of the noncanonical NF-kappa B pathway. *J. Biol. Chem.* **282**, 3688–3694 (2007).
- Vaahromeri, K. et al. Locally triggered release of the chemokine CCL21 promotes dendritic cell transmigration across lymphatic endothelia. *Cell Rep.* **19**, 902–909 (2017).
- Mackay, C. R., Marston, W. L. & Dudler, L. Naive and memory T cells show distinct pathways of lymphocyte recirculation. *J. Exp. Med.* **171**, 801–817 (1990).
- Srinivasan, R. S. et al. Lineage tracing demonstrates the venous origin of the mammalian lymphatic vasculature. *Genes Dev.* **21**, 2422–2432 (2007).
- Wimmer, N. et al. Lymphotoxin beta receptor activation on macrophages induces cross-tolerance to TLR4 and TLR9 ligands. *J. Immunol.* **188**, 3426–3433 (2012).
- Fontenot, J. D. et al. Regulatory T cell lineage specification by the forkhead transcription factor foxp3. *Immunity* **22**, 329–341 (2005).
- Pace, C. N., Vajdos, F., Fee, L., Grimley, G. & Gray, T. How to measure and predict the molar absorption coefficient of a protein. *Protein Sci.* **4**, 2411–2423 (1995).
- Lutz, M. B. et al. An advanced culture method for generating large quantities of highly pure dendritic cells from mouse bone marrow. *J. Immunol. Methods* **223**, 77–92 (1999).
- Robbiani, D. F. et al. The leukotriene C(4) transporter MRP1 regulates CCL19 (MIP-3beta, ELC)-dependent mobilization of dendritic cells to lymph nodes. *Cell* **103**, 757–768 (2000).

Acknowledgements

This work was supported by NIH grant PHS RO1 AI062765 to J.S.B. and the Maryland Living Legacy Foundation to J.S.B. and W.P.

Author contributions

W.P. and J.S.B. designed the research. W.P., Y.X., L.L., N.T., and C. W. performed the experiments. K.F. performed bioinformatics and statistical analyses. V.S. and T.S. provided critical material and reagents. W.P., Y.X., C.C.B., and J.S.B. analyzed the results. W. P. and J.S.B. wrote the manuscript.

Additional information

Supplementary Information accompanies this paper at <https://doi.org/10.1038/s41467-018-05412-0>.

Competing interests: The authors declare no competing interests.

Reprints and permission information is available online at <http://npg.nature.com/reprintsandpermissions/>

Publisher's note: Springer Nature remains neutral with regard to jurisdictional claims in published maps and institutional affiliations.



Open Access This article is licensed under a Creative Commons Attribution 4.0 International License, which permits use, sharing, adaptation, distribution and reproduction in any medium or format, as long as you give appropriate credit to the original author(s) and the source, provide a link to the Creative Commons license, and indicate if changes were made. The images or other third party material in this article are included in the article's Creative Commons license, unless indicated otherwise in a credit line to the material. If material is not included in the article's Creative Commons license and your intended use is not permitted by statutory regulation or exceeds the permitted use, you will need to obtain permission directly from the copyright holder. To view a copy of this license, visit <http://creativecommons.org/licenses/by/4.0/>.

© The Author(s) 2018